Narrow Low-Frequency Spectrum and Heat Management by Thermocrystals

Martin Maldovan

Department of Materials Science and Engineering, Massachusetts Institute of Technology, 77 Massachusetts Avenue, Cambridge, Massachusetts 02139, USA

(Received 6 September 2012; published 9 January 2013)

By transforming heat flux from particle to wave phonon transport, we introduce a new class of engineered material to control thermal conduction. We show that rationally designed nanostructured alloys can lead to a fundamental new approach for thermal management, guiding heat as photonic and phononic crystals guide light and sound, respectively. Novel applications for these materials include heat waveguides, thermal lattices, heat imaging, thermo-optics, thermal diodes, and thermal cloaking.

DOI: 10.1103/PhysRevLett.110.025902 PACS numbers: 65.80.−g, 43.40.+s, 63.20.−e, 66.70.Lm

The ability to manipulate heat flow is essential in the development of many technological devices such as thermoelectrics [1–3], nano- and optoelectronics [4], fuel cells [5], solar cells [6], thermal barrier coatings [7], and low thermal conductivity materials [8]. Traditional techniques to control thermal energy flow have been based on introducing impurities, defects, and alloy atoms in the crystal lattice. In recent years, however, many alternative methods have been developed and several nanostructures and complex compounds are used intensely to control heat transport by means of guest atoms and phonon interface scattering [1–3,8–12]. Here, we introduce a new class of thermal material, called a ''thermocrystal,'' that can manipulate the flow of thermal energy by exploiting the coherent reflection of phonons from internal surfaces. By engineering the phonon spectrum, we transform heat flow from its standard form as diffusive particles to wave phonon transport. Our results show that the 2D patterning of nanostructured alloys can lead to a radical new departure on thermal energy management, guiding heat as photonic and phononic crystals guide light and sound, respectively. The results lay the foundation for creating heat waveguides, thermal lattices, heat imaging, thermo-optics, thermal diodes, and thermal cloaking.

In order to manage thermal energy flow in semiconductors, considerable attention has recently turned to nanostructures such as thin films, nanowires, and superlattices [1–3,8–10], and to open crystal structures such as skutterudites and clathrates [11,12]. In nanostructures, the thermal conductivity κ is reduced by the shortening of the phonon mean-free paths through diffuse interface scattering. In open crystals, guest atoms filling the lattice nanocages decrease κ by acting as atomic ''rattlers'' or through quasiharmonic guest-lattice coupling [11,12]. It has been suggested that coherent interference influences κ in superlattices [13,14]. However, it was indicated that diffuse interface scattering partially or totally prevails over coherent interference and thermal transport is also dominated by incoherent scattering [1,15,16]. Coherent interference have also been ascribed to the reduced thermal conductivity of nanomeshes [16] but thermal phonon wavelengths are 1 order of magnitude smaller than the nanomesh periodicity, preventing effective coherent effects [17–19]. We report here a new class of thermal material that can control the flow of thermal energy by manipulating the interference of ''heat waves.'' We note that heat and sound are both mechanical vibrations of the atomic lattice, where large wavelengths correspond to sound and short wavelengths to heat. Sound wave propagation can be coherently managed by phononic crystals [19], which are periodic structures made of two elastic materials, where vibrations with wavelengths λ comparable to the periodicity a can be controlled in many useful ways due to the existence of forbidden frequency gaps. If we consider using phononic crystals to control heat in semiconductors such as silicon, where thermal phonon wavelengths are $\sim$1–10 nm [17], the structure periodicity should be $a \sim 2$ nm [18]. This scale is extremely difficult to realize in practice. We propose here to transform thermal energy flow from its standard form as short-wavelength particle transport to long-wavelength wave transport. This ''hypersonic heat'' is an unexplored heat transport mode with fundamental and practical relevance that can be manipulated by designing appropriate periodic structures. We note that thermal flow must not only be carried by long-wavelength phonons but also considerably reduced to a specific range that corresponds to the frequency gap created by the underlying thermocrystal.

We introduce next the scheme to create a flow of thermal energy carried by phonons with specific frequencies (heat spectrum engineering), which involves alloy atoms, nanoparticles, and boundary size effects. Without losing generality, we consider silicon as the material we want to transform into a thermocrystal. Figure 1 shows that in bulk silicon heat is primarily carried by phonons with frequencies f higher than 1 THz [17]. To increase the proportion of heat carried by low-frequency (< 1 THz) phonons, we first consider a $Si_{1-x}Ge_x$ alloy lattice, where the mass-difference scattering ($\sim \omega^4$) efficiently blocks high-frequency phonons without significantly altering

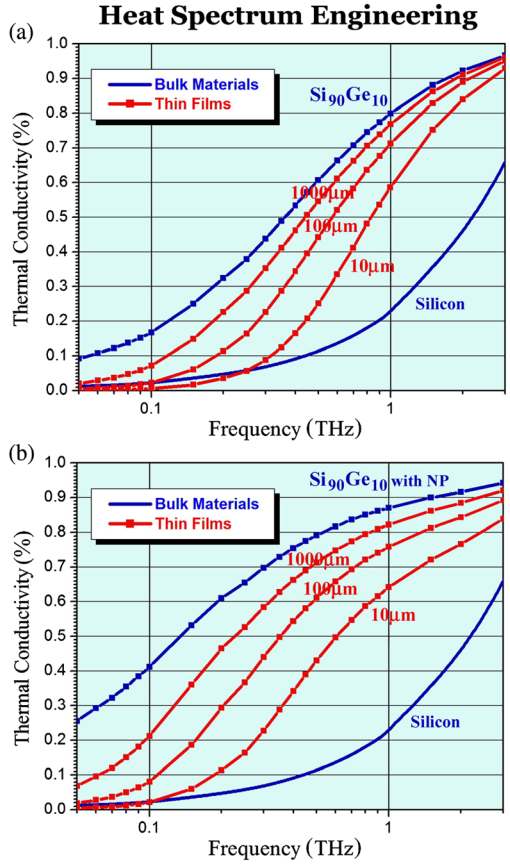

FIG. 1 (color online). Cumulative κ as a function of frequency for (a) $Si_{90}Ge_{10}$ and (b) nanoparticle $Si_{90}Ge_{10}$. Blue lines correspond to bulk materials and red lines to thin film samples with thicknesses $t = 1000$, 100, and 10 μm, respectively. The cumulative κ for bulk silicon is shown as reference. For $Si_{90}Ge_{10}$, $\kappa =$ 20, 18, 14, and 10 W/(m°K) for bulk, $t = 1000$, 100, and 10 μm, respectively. For nanoparticle $Si_{90}Ge_{10}$, the numbers are $\kappa = 7$, 5, 3.7, and 2.5 W/(m°K).

low-frequency phonons. This reduces κ, but more importantly, it shifts heat transport to lower frequencies. To further enhance the low-frequency proportion, we also consider the introduction of Ge nanoparticles within the $Si_{1-x}Ge_x$ alloy. The nanoparticle approach has recently been demonstrated to efficiently reduce κ in thermoelectrics [20–22]. When the nanoparticle size is small enough, the scattering strength for high-frequency phonons is significantly higher than that for low-frequency phonons, providing an additional mechanism to shift heat transport to lower frequencies. We note that efficient thermoelectrics require maximal thermal conductivity reduction by scattering the larger number of phonon wavelengths [20–22]. In contrast, the goal in our paper is to scatter specific short and very large phonon wavelengths such that heat can be carried by a narrow frequency band.

For boundary size effects, we employ a theoretical model based on the Boltzmann transport equation (BTE), which we have used previously to obtain the thermal conductivity of nanowires, thin films, and polycrystals, and found good agreement with experiments [23–26]. Under the relaxation time approximation, κ can be calculated by the formulas [23–27]

$$\kappa(T) = \oint \sum_j \sum_{\vec{\mathbf{k}}} k_B \left[\frac{\hbar\omega_j(\vec{\mathbf{k}})}{k_B T}\right]^2 \times \frac{\exp(\hbar\omega_j(\vec{\mathbf{k}})/k_B T)}{[\exp(\hbar\omega_j(\vec{\mathbf{k}})/k_B T) - 1]^2} \cos^2\theta \nu_j(\vec{\mathbf{k}}) \ell_j(\vec{\mathbf{k}}) dS, \quad (1)$$

with

$$\ell_j(\vec{\mathbf{k}}) = \ell_{0j}(\vec{\mathbf{k}}) \left[1 - \frac{[1 - p(\vec{\mathbf{k}})]\exp[-L_1(\vec{\mathbf{k}})/\ell_{0j}(\vec{\mathbf{k}})]}{1 - p(\vec{\mathbf{k}})\exp[-L_2(\vec{\mathbf{k}})/\ell_{0j}(\vec{\mathbf{k}})]}\right], \quad (2)$$

where $\hbar$ and k_B are the Planck and Boltzmann constants, T is the temperature, $\omega_j(\mathbf{k})$ is the dispersion relation, $\nu_j(\mathbf{k}) = \nabla_{\mathbf{k}}\omega_j(\mathbf{k})$ is the group velocity, $\ell_{0j}(\mathbf{k})$ and $\ell_j(\mathbf{k})$ are the bulk and reduced phonon mean-free paths, respectively, j are different polarizations, $p(\mathbf{k})$ is the boundary specularity, $L_1(\mathbf{k})$ and $L_2(\mathbf{k})$ are characteristic lengths, and θ is the angle between the wave vector $\mathbf{k}$ and the gradient ∇T. $\kappa(T)$ is integrated over the cross section dS and over all Brillouin wave vectors $\mathbf{k}$. We note that using Eqs. (1) and (2) is *equivalent* to solving the BTE analytically, as done in the well-known Fuchs and Sondheimer formulations [28,29]. We also note that Eq. (2) replaces the commonly used Matthiessen's rule by correctly considering boundary scattering as a surface effect [27].

The bulk mean-free paths $\ell_{0j}(\mathbf{k}) = \nu_j(\mathbf{k})\tau_{0j}(\mathbf{k})$, where $\tau_{0j}(\mathbf{k})$ is the relaxation time, are calculated by considering scattering by phonons, isotopes, alloy atoms, and nanoparticles. By separately considering longitudinal (LA) and transverse (TA) acoustic polarizations, we obtain the phonon-phonon relaxation times for Si by comparing Boltzmann calculations to the experimental bulk thermal conductivity. The relaxation times are $[\tau^{\text{eff}}_{0,\text{LA}}(\omega)]^{-1} = B(T)\omega^2$, $[\tau^{\text{eff}}_{0,\text{TA}}(\omega)]^{-1} = (1/4)B(T)\omega^2$, with $B(T) = 3.28 \times 10^{-19} T \exp(-140/T)$ s/K [24]. We note that the above phonon-phonon relaxation times show reasonable good agreement across the entire frequency spectrum with those calculated from first-principles approaches [30]. The scattering rates for $Si_{1-x}Ge_x$ alloys are well described by effective medium approaches, where Rayleigh scattering is calculated by considering either a Si or Ge atom embedded in a medium with average properties [21,27,31]. This approach correctly represents the dependence of κ on $Si_{1-x}Ge_x$ alloy composition [21,31–33]. The scattering rates for $Si_{1-x}Ge_x$ alloys $\tau^{-1}_{\text{alloy}} = x(1-x)3.01 \times 10^{-41}\omega^4$ are from Refs. [21,32]. For scattering rates due to nanoparticles (np) $\tau^{-1}_{\text{np}} = v(\sigma_s^{-1} + \sigma_l^{-1})^{-1}\rho_{\text{np}}$ we consider interpolation between long- and short-wavelength scattering regimes, with $\sigma_l = \pi R^2(4/9)(\Delta d/d)^2(\omega R/v)^4$ and $\sigma_s = 2\pi R^2$, where ρ_{np} is the nanoparticle density, Δd is the particle-matrix density difference, and d is the matrix

density. As it is well known, the short-wavelength scattering limit is twice the particle cross section, while the long-wavelength limit is three times the Rayleigh expression. The details about the nanoparticle scattering approach can be found in Ref. [21].

Figure 1(a) shows the cumulative thermal conductivity for $Si_{90}Ge_{10}$ bulk alloys at $T = 300$ K, where the phonon frequency balance has been strongly modified due to the frequency dependence of alloy scattering ($\sim \omega^4$), e.g., phonons with frequencies $f > 1$ THz carry ~80% of the heat in bulk Si but ~20% in a $Si_{90}Ge_{10}$ alloy. For a nanostructured $Si_{90}Ge_{10}$ bulk alloy, we consider embedding Ge nanoparticles with small diameters $d \sim 1$ nm and 10% filling fraction to selectively block high-frequency phonons. Figure 1(b) displays the corresponding cumulative thermal conductivity, where thermal transport is further shifted to lower frequencies due to the presence of the nanoparticles. As Fig. 1 clearly shows, alloying and nanoparticle inclusions are effective mechanisms to greatly increase the proportion of heat transported by low-frequency phonons. We note that in contrast to thermoelectrics [20–22], we have selectively blocked very high-frequency phonons.

In terms of thermocrystals, our next objective is to reduce the contribution of *very* low-frequency phonons in order to concentrate heat transport around a specific frequency range that can be managed by a purposely designed periodic structure. To achieve this, we propose using thin films with rough surface boundaries where the film thicknesses are larger than the mean-free paths of medium- and high-frequency phonons. In this manner, only very low-frequency phonons are subject to significant size effects and their contributions to κ reduced. We show in Figs. 1(a) and 1(b) the heat spectra for $Si_{90}Ge_{10}$ and nanoparticle $Si_{90}Ge_{10}$ *thin films* with thicknesses $t = 10$, 100, and 1000 μm respectively, where the very low-frequency contribution is greatly reduced with respect to bulk materials. Note that by engineering the phonon spectrum, we are able to concentrate most of the heat spectra to a relatively low-frequency window ~0.1 THz $< f <$ ~2.0 THz with up to ~40% of the heat restricted to a narrow "hypersonic" 100–300 GHz range. In addition, because of boundary scattering, thermal transport is primarily due to phonons propagating close to the film plane, e.g., for nanoparticle $Si_{90}Ge_{10}$ films with $t = 100$ and 1000 μm, ~71% and ~80% of heat is carried by phonons with angles less than 30°. Moreover, thermal phonons in the films propagate relatively large distances due to the low frequencies involved; e.g., in nanoparticle $Si_{90}Ge_{10}$, phonon mean-free paths are ~200–700 μm.

We next introduce purposely designed periodic structures to manage these heat carrying hypersonic modes created by phonon spectrum engineering. The dispersion relations for elastic waves in thermocrystals made of $Si_{90}Ge_{10}$ and nanostructured $Si_{90}Ge_{10}$ thin films (Fig. 2) are obtained by using the finite element method to solve the elastic wave equation [18,19,34,35]

$$\rho \frac{\partial^2 u_i}{\partial t^2} = \nabla \cdot (\rho c_t^2 \nabla u_i) + \nabla \cdot \left(\rho c_t^2 \frac{\partial \mathbf{u}}{\partial x_i} \right) + \frac{\partial}{\partial x_i} [(\rho c_l^2 - 2\rho c_t^2) \nabla \cdot \mathbf{u}], \quad (3)$$

where $\mathbf{u}$ is the displacement, ρ is the density, and c_t, c_l are the transverse and longitudinal velocities. We note that because heat is made of both particle and wave phonons, we use the wave equation [Eq. (3)] to describe phonon wave properties (hypersonic frequencies) whereas we use the Boltzmann transport equation [Eq. (1)] to describe particle phonons (high and very low frequencies), the basic idea being to reduce the diffuse particle contribution to enhance the wave properties of heat transport. Note that the air holes will not give rise to significant diffuse interface scattering for the hypersonic modes. This is because the phonon wavelengths ($\lambda \sim 2a$) are much larger than the surface roughness of the air holes. The influence of the air holes is taken into account by the wave equation [Eq. (3)] through specular surface reflections. Also note that the air holes will additionally reduce high-frequency contributions, increasing the thermocrystal efficiency. Figures 2(a) and 2(b) show the phononic band gaps (yellow) that correspond to $Si_{90}Ge_{10}$ and nanostructured $Si_{90}Ge_{10}$ films patterned with a square arrangement of air cylinders (S1) [18] and with a complex but more effective design (S2) [35]. Figures 2(c) and 2(d) show the (S1) thermocrystal thin film and the corresponding band diagram for a nanoparticle $Si_{90}Ge_{10}$ matrix. The yellow area indicates the phononic band gap, which is designed to correspond to heat carrying hypersonic frequencies. The structure periodicities are $a \sim$ 10–20 nm, which are accessible with current experimental techniques. We note that in nanostructured $Si_{90}Ge_{10}$ films, up to 23% of thermal transport is carried by phonons with frequencies in the gaps. In particular, for the S1 sample, 16% and 18% of the heat spectrum corresponds to band gap frequencies when $a =$ 10 and 20 nm, respectively. These values increase to 21% and 23% in the case of the S2 sample. For the $Si_{90}Ge_{10}$ films, the values decrease to 15% and 9% for the S1 sample, and 22% and 13% for the S2 sample. We note that, if the samples are made of silicon, only ~2%–4% of heat transport corresponds to gap frequencies. Importantly, the phonon mean-free paths are orders of magnitude larger than the structure periodicities, which is a critical additional requirement to achieve effective interference effects. We have therefore concentrated the heat spectrum to a specific frequency range that is compatible with a phononic crystal that can be fabricated. This means that the propagation of thermal phonons in nanostructured alloy films can be managed through coherent interference effects. While in the past phononic crystals have been shown to manage sound waves, these are the first phononic crystals rationally designed to manage heat-carrying phonon modes. This can have an unprecedented impact in thermal management as heat transport can now be engineered by the rational design of periodic structures.

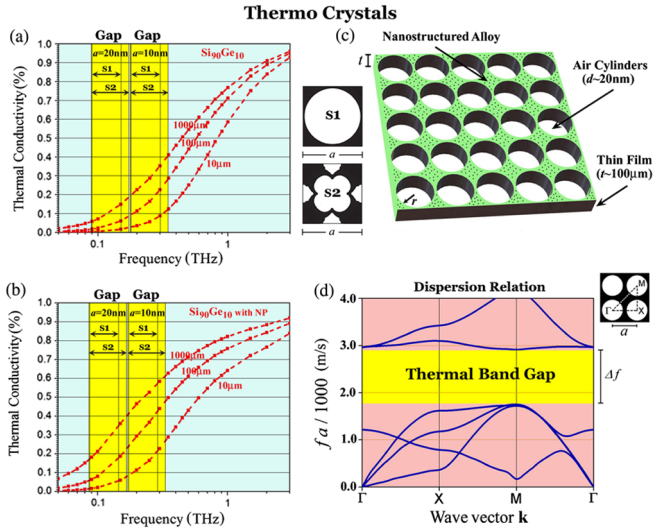

FIG. 2 (color online). (a) and (b) Yellow areas show the frequency gaps corresponding to the films patterned with a square arrangement of air cylinders (S1) [18] and with a complex but more effective design (S2) [35]. The lattice constants are 10 nm (right) and 20 nm (left). (c) Schematic of a thermocrystal made of a periodic array of air cylinders patterned on a nanostructured alloy film. (d) The corresponding phononic band diagram for a thermocrystal made of nanoparticle $Si_{90}Ge_{10}$ with cylinder radius $r/a = 0.48$, where phonon frequencies are plotted versus the wave vector $\mathbf{k}$. The thermocrystals are designed such that the gap frequencies (yellow area) correspond to heat modes.

We note that further improvements can be achieved by using impurities, dislocations, guest atoms, and/or amorphism to block high-frequency phonons and also grain boundaries and/or interfaces to block very low-frequency phonons. The current search for large phononic band gap materials will also be important for highly efficient thermocrystals. The structure and processing technique that will prevail in the future will be the one with the best compromise between efficiency and ease of fabrication.

By analogy with photonics and phononics, these results open up opportunities and future challenges for novel and exciting ways to control thermal energy flow, which we briefly summarize below. In contrast to photonics and phononics, however, the goal in thermal management is *not* to guide a single frequency mode. In fact, all guided or localized phonon modes are expected to be excited. We also note that the proposed applications have *all* been demonstrated for sound [36–43]; the challenge is to transform these applications to heat-carrying phonon modes by employing the rationale described in our paper: (1) *Heat waveguides*: Once we have a thermocrystal with a frequency gap comprising a significant part of the heat spectrum, it would be interesting to introduce a line defect. Hypersonic heat modes would thus be guided by the presence of the channel and directed along the direction of the waveguide [see Fig. 3(a)] [36,44]. (2) *Thermal lattices*: One can also introduce point defects in a thermocrystal to localize hypersonic heat modes at particular places. This can be done by removing individual air cylinders [18,44] and can result in a thermally activated lattice of confined heat modes [see Fig. 3(b)]. (3) *Heat imaging*: Periodic air-solid structures can create negative refraction of elastic waves [37], which allows the fabrication of flat acoustic superlenses [see Fig. 3(c)]. It would be interesting to design thermocrystals such that the frequency ranges for negative refraction match the hypersonic heat frequencies. In this manner, hypersonic heat modes from a source at a distance from the negative-refractive interface will form an image on the right-hand side [37,38]. (4) *Thermo-optics*: Air-silicon periodic structures can also simultaneously

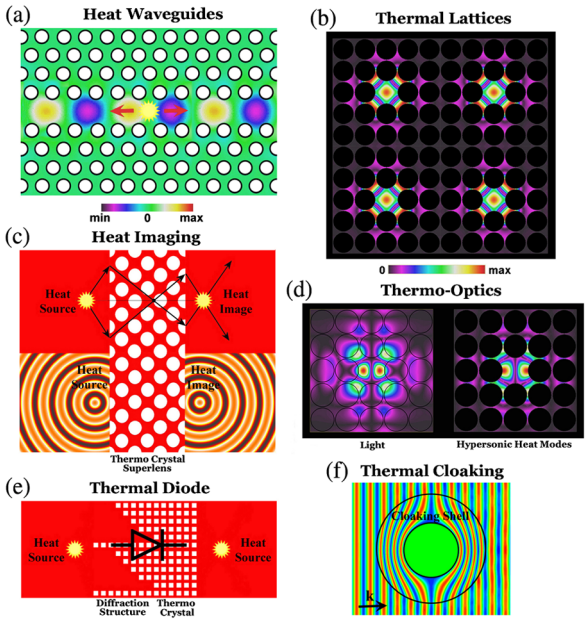

FIG. 3 (color online). Schematics for thermocrystals opportunities and challenges (a) *Heat waveguides*: A waveguide is created in a triangular lattice of air rods (white). Hypersonic heat modes (yellow) can be guided along the channel. Color scheme shows the displacement field for a hypersonic wave propagating in the waveguide. (b) *Thermal lattices*: Point defects are introduced in a square lattice of air rods (black) [18]. Hypersonic heat modes can be localized around the defects. Color scheme shows time averaged displacement fields for confined modes. (c) *Heat imaging*: Schematic of a heat source and its image across a thermocrystal superlense. Negative refracted [37] hypersonic beams (black arrows) focus the point source (yellow) located on one side of the lens into a real image on the other side. (d) *Thermo-optics*: A point defect in a thermocrystal (missing cylinder) can localize both light and hypersonic heat modes and enhance light-heat interactions. Color scheme shows time averaged fields for localized photon (left) and phonon (right) modes. (e) *Thermal diode*: Schematic of a diode made of a diffraction structure and a periodic array of cylinders [42]. Hypersonic heat modes from the right have smaller transmission than those from the left. The system can provide thermal rectification through nonreciprocal phonon propagation. (f) *Thermal cloaking*: Acoustic pressure field for a cylindrical scatterer surrounded by a cloaking shell (adapted from Ref. [43]). The development of metamaterials for elastic waves can lead to low temperature thermal cloaking.

localize light and sound [18] and enhance light-matter interactions [39,40]. Light trapping requires $a \sim 100$ nm, which in turn localizes hypersonic modes with $f \sim 10$ GHz [see Fig. 3(d)]. These frequencies are relatively low for room temperature Si-based thermocrystals, but lower temperatures and/or other materials can be considered to achieve new methods of probing, stimulating, and using optical-heat interactions in chip-scale platforms [18,39,40]. (5) *Thermal diodes*: Nonreciprocal wave propagation typically requires nonlinear materials [41]. Acoustic diodes, however, were recently demonstrated by broken inversion symmetry in phononic crystals [42]. The application of this phenomenon to hypersonic modes in thermocrystals can lead to thermal devices that enable thermal rectification through nonreciprocal phonon transport [41,42]. (6) *Thermal cloaking*: Electromagnetic and acoustic cloaking have been recently demonstrated through metamaterials [43]. More challenging, however, has been the design of an elastic cloaking. The development of elastic metamaterials can lead to thermal cloaking at low temperatures where heat is carried by wavelengths larger than typical metamaterial scales and diffuse Fourier transport does not apply [45].

In conclusion, by transforming heat flux from particle to wave phonon transport, we have introduced a new class of engineered material to control thermal conduction. We showed that rationally designed nanostructured alloy films can lead to a fundamental new approach for thermal management, guiding heat as photonic and phononic crystals guide light and sound, respectively. Thermocrystals thus offer the possibility of initiating significant new developments by introducing many novel thermal effects and devices.

[1] R. Venkatasubramanian, E. Siivola, T. Colpitts, and B. O'Quinn, Nature (London) **413**, 597 (2001).
[2] A. I. Hochbaum, R. Chen, R. D. Delgado, W. Liang, E. C. Garnett, M. Najarian, A. Majumdar, and P. Yang, Nature (London) **451**, 163 (2008).
[3] A. I. Boukai, Y. Bunimovich, J. Tahir-Kheli, J.-K. Yu, W. A. Goddard, and J. R. Heath, Nature (London) **451**, 168 (2008).
[4] B. Tian, X. Zheng, T. J. Kempa, Y. Fang, N. Yu, G. Yu, J. Huang, and C. M. Lieber, Nature (London) **449**, 885 (2007).
[5] B. C. H. Steele and A. Heinzel, Nature (London) **414**, 345 (2001).
[6] P. Wang, S. M. Zakeeruddin, J. E. Moser, M. K. Nasseruddin, T. Sekiguchi, and M. Gratzel, Nat. Mater. **2**, 402 (2003).
[7] N. P. Padture, M. Gell, and E. H. Jordan, Science **296**, 280 (2002).
[8] C. Chiritescu, D. G. Cahill, N. Nguyen, D. Johnson, A. Bodapati, P. Keblinski, and P. Zschack, Science **315**, 351 (2007).
[9] K. F. Hsu, S. Loo, F. Guo, W. Chen, J. S. Dyck, C. Uher, T. Hogan, E. K. Polychroniadis, and M. G. Kanatzidis, Science **303**, 818 (2004).
[10] B. Poudel, Q. Hao, Y. Ma, Y. Lan, A. Minnich, B. Yu, X. Yan, D. Wang, A. Muto, D. Vashaee, X. Chen, J. Liu, M. S. Dresselhaus, G. Chen, and Z. Ren, Science **320**, 634 (2008).
[11] B. C. Sales, D. Mandrys, and R. K. Williams, Science **272**, 1325 (1996).
[12] M. M. Koza, M. R. Johnson, R. Viennois, H. Mutka, L. Girard, and D. Ravot, Nat. Mater. **7**, 805 (2008).
[13] R. Venkatasubramanian, Phys. Rev. B **61**, 3091 (2000).
[14] M. V. Simkin and G. D. Mahan, Phys. Rev. Lett. **84**, 927 (2000).
[15] B. Yang and G. Chen, Phys. Rev. B **67**, 195311 (2003).
[16] J. K. Yu, S. Mitrovic, D. Tham, J. Varghese, and J. R. Heath, Nat. Nanotechnol. **5**, 718 (2010).
[17] A. J. Minnich, M. S. Dresselhaus, Z. F. Ren, and G. Chen, Energy Environ. Sci. **2**, 466 (2009).
[18] M. Maldovan and E. L. Thomas, Appl. Phys. Lett. **88**, 251907 (2006).
[19] M. S. Kushwaha, P. Halevi, L. Dobrzynski, and B. Djafari-Rouhani, Phys. Rev. Lett. **71**, 2022 (1993).
[20] W. Kim, J. Zide, A. Gossard, D. Klenov, S. Stemmer, A. Shakouri, and A. Majumdar, Phys. Rev. Lett. **96**, 045901 (2006).
[21] N. Mingo, D. Hauser, N. P. Kobayashi, M. Plissonnier, and A. Shakouri, Nano Lett. **9**, 711 (2009).
[22] K. Biswas, J. He, I. D. Blum, C.-I Wu, T. P. Hogan, D. N. Seidman, V. P. Dravid, and M. G. Kanatzidis, Nature (London) **489**, 414 (2012).
[23] M. Maldovan, J. Appl. Phys. **110**, 034308 (2011).
[24] M. Maldovan, J. Appl. Phys. **110**, 114310 (2011).
[25] M. Maldovan, J. Appl. Phys. **111**, 024311 (2012).
[26] M. Maldovan, Appl. Phys. Lett. **101**, 113110 (2012).
[27] J. M. Ziman, *Electrons and Phonons* (Cambridge University Press, London, England, 2001).
[28] K. Fuchs, Proc. Cambridge Philos. Soc. **34**, 100 (1938).
[29] E. H. Sondheimer, Adv. Phys. **1**, 1 (1952).
[30] K. Esfarjani, G. Chen, and H. T. Stokes, Phys. Rev. B **84**, 085204 (2011).
[31] B. Abeles, Phys. Rev. **131**, 1906 (1963).
[32] Z. Wang and N. Mingo, Appl. Phys. Lett. **97**, 101903 (2010).
[33] H. Kim, I. Kim, I. Choi, and W. Kim, Appl. Phys. Lett. **96**, 233106 (2010).
[34] M. Maldovan and E. L. Thomas, Appl. Phys. B **83**, 595 (2006).
[35] O. R. Bilal and M. I. Hussein, Phys. Rev. E **84**, 065701 (2011).
[36] A. Khelif, B. Djafari-Rouhani, J. O. Vasseur, and P. A. Deymier, Phys. Rev. B **68**, 024302 (2003).
[37] A. C. Hladky-Hennion, J. Vasseur, B. Dubus, B. Djafari-Rouhani, D. Ekeom, and B. Morvan, J. Appl. Phys. **104**, 064906 (2008).
[38] X. Zhang and Z. Liu, Appl. Phys. Lett. **85**, 341 (2004).
[39] M. Eichenfield, J. Chan, R. M. Camacho, K. J. Vahala, and O. Painter, Nature (London) **462**, 78 (2009).
[40] J. Chan, T. P. Mayer Alegre, A. H. Safani-Naeini, J. T. Hill, A. Krause, S. Groblacher, M. Aspelmeyer, and O. Painter, Nature (London) **478**, 89 (2011).
[41] B. Liang, X. S. Guo, J. Tu, D. Zhang, and J. C. Cheng, Nat. Mater. **9**, 989 (2010).
[42] X. F. Li, X. Ni, L. Feng, M-H. Lu, C. He, and Y-F Chen, Phys. Rev. Lett. **106**, 084301 (2011).
[43] D. Torres and J. Sanchez-Dehesa, New J. Phys. **10**, 063015 (2008).
[44] J. D. Joannopoulos, P. R. Villeneuve, and S. Fan, Nature (London) **386**, 143 (1997).
[45] S. Narayana and Y. Sato, Phys. Rev. Lett. **108**, 214303 (2012).